Electronic Supplementary Material (ESI) for Biomaterials Science.
This journal is © The Royal Society of Chemistry 2019

Supporting Information for:

A Near Infrared-Modulated Thermosensitive Hydrogel for Stabilization of Indocyanine Green and Combinatorial Anticancer Phototherapy

Chanjuan Liu [a,b], Changping Ruan [a], Rui Shi [a], Bang-Ping Jiang [a], Shichen Ji [a], Xing-Can Shen [a,*]

[a] State Key Laboratory for Chemistry and Molecular Engineering of Medicinal Resources, School of Chemistry and Pharmaceutical Science, Guangxi Normal University, Guilin, 541001, China.

[b] Key Laboratory of New Processing Technology for Nonferrous Metal & Materials, Ministry of Education, and School of Material Science and Engineering, Guilin University of Technology, Guilin 541004, P. R. China.

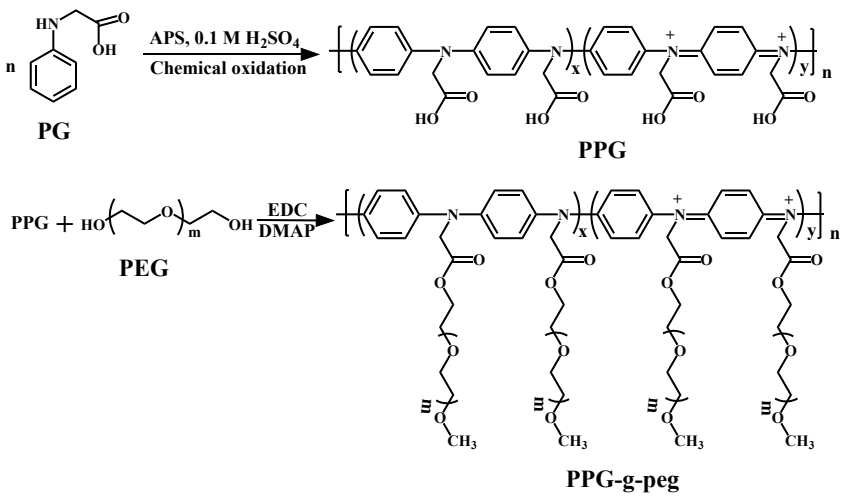

Scheme S1. Synthesis routs for the PPG-g-peg photothermal backbone.

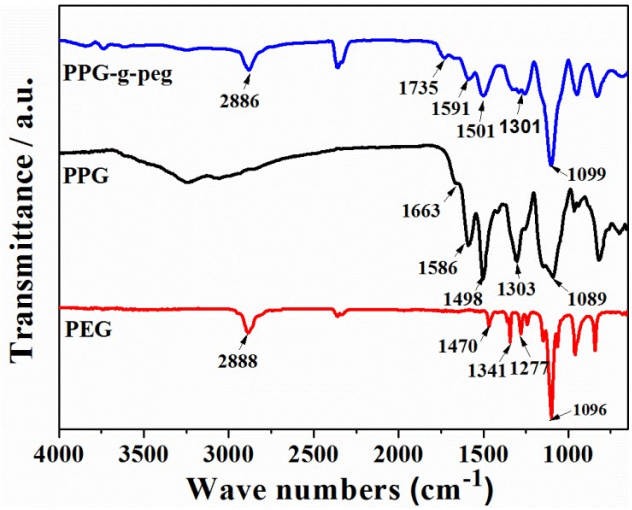

Figure S1. FT-IR spectrum of PPG-g-peg compared with PEG and PPG. For PPG-g-peg, the bands at 1501 and 1591 cm^{-1} were related to stretching band of the benzenoid and quinoid rings of PPG main chain.[1] The C–O–C stretching vibration and the $–CH_2–$ stretching vibration for PEG side chain were located at 1099 cm^{-1} and 2886 cm^{-1}, respectively. Most importantly, the peak located at 1735 cm^{-1} corresponded to the C=O stretching vibration absorption of ester bone connecting PPG and PEG was also clearly seen. These analysis supporting the successful synthesis of PPG-g-peg.

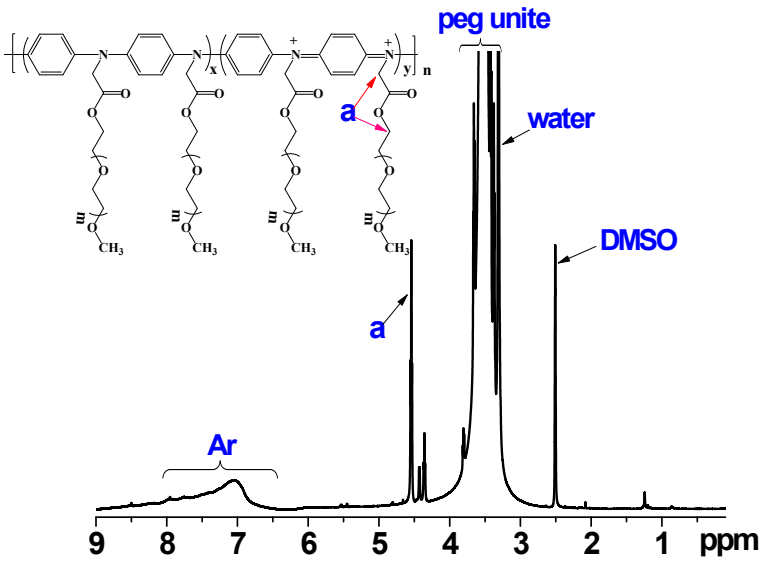

Figure S2. ^{1}H NMR spectrum of PPG-g-peg dissolved in DMSO-d_6. The charactristic signals of aromatic ring protons belong to PPG backbone located at the range of 6.41 ~ 8.10 ppm, and the typical proton peaks presented at 3.12 ~ 4.04 ppm which were contributed to the methylene unite of peg side chains. Moreover, the signals observed at 4.52 ~ 4.55 ppm were ascribed to the methylene "a", which located on both sides of the ester group in the side chain.

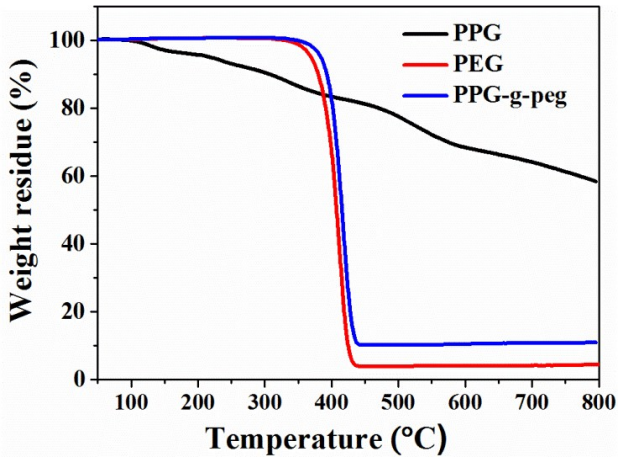

Figure S3. TGA curves of PEG, PPG and PPG-g-peg. It was obviously noted that the PPG had excellent thermal stability due to the rigid aromatic ring chain, while the flexible aliphatic hydrocarbon PEG chain exhibited lower thermal performance. And the heat-resistant performance of PPG-g-peg grafted polymer was between pristine PPG and PEG. The onset decomposition temperature of PPG-g-peg (382 °C) is higher than that of pristine PEG (369 °C) due to the introduction of rigid PPG chain. Moreover**,** the PPG-g-peg had an 89.0% weight loss at 800 °C, while the values for PEG and PPG were 95.6% and 41.6%, respectively. The ratio of PPG and PEG was estimated according to the following equation.[2]

$$0.96x + 0.42y = 0.89 \quad (1)$$

$$x + y = 1 \quad (2)$$

x and y are weight percentage of PEG and PPG, respectively. $x = 87.3\%$, and the grafting ratio of PEG to PG unit is determined to be 26.0 %.

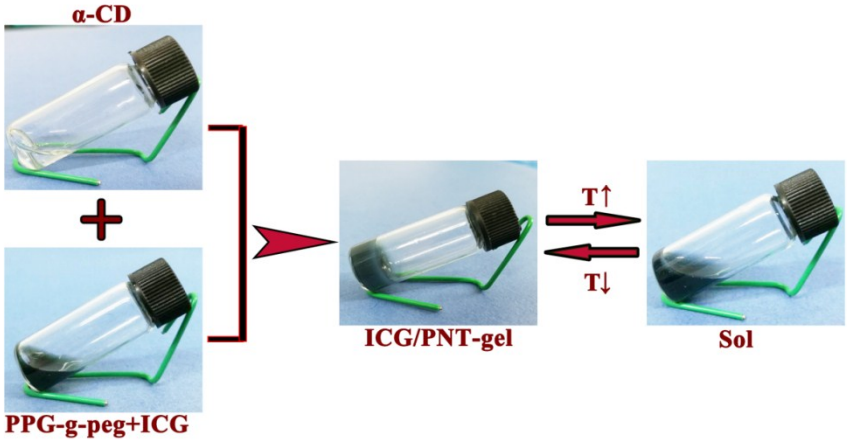

Figure S4. Digital photos of formation process and thermo-sensitive gel-sol transition of ICG/PNT-gel.

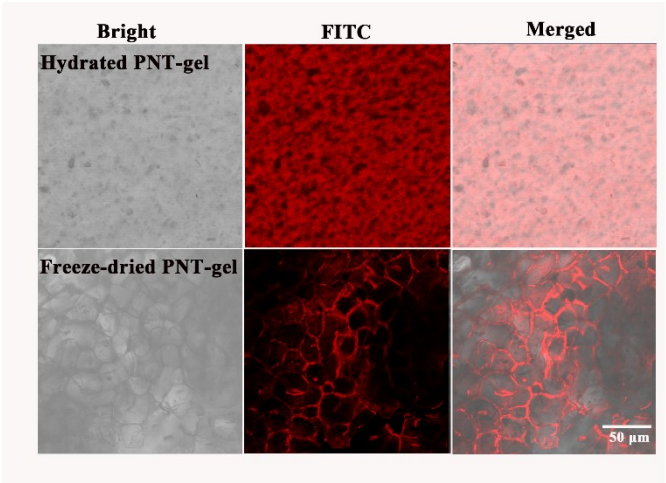

Figure S5. Confocal laser scanning fluorescence micrographs of PNT-gel networks (stained with FITC) in the hydrated state and freeze-dried stated, respectively.

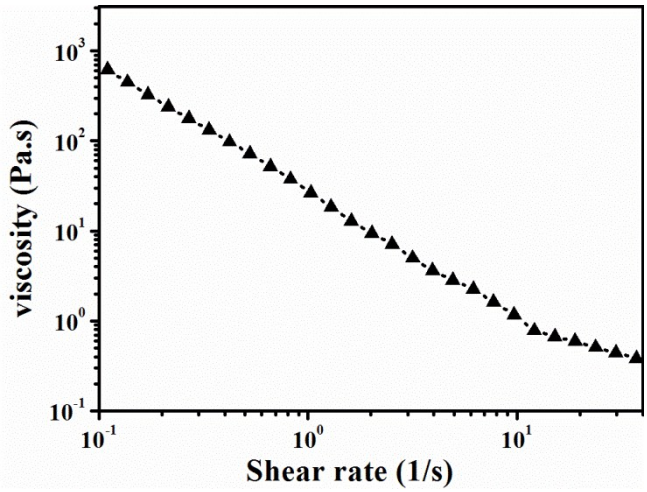

Figure S6. The shear-dependent viscosity of the PNT-gel.

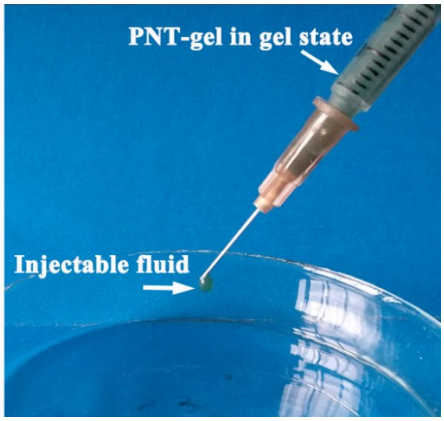

Figure S7. Digital photograph of injectable PNT-gel and its shear-thinning property.

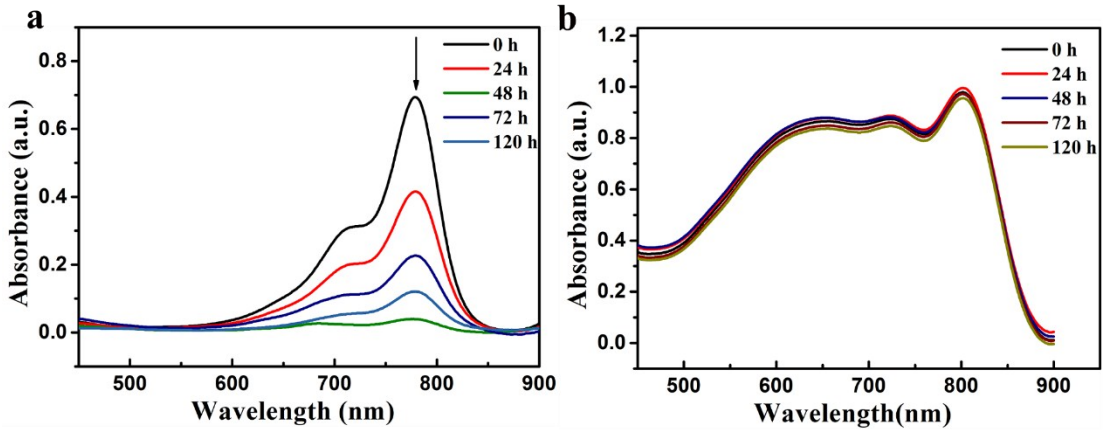

Figure S8. Stability investigation of free ICG and ICG/PPG-g-peg complex. UV-vis-NIR absorbance spectra of (a) free ICG and (b) ICG/PPG-g-peg complex after storage at room temperature.

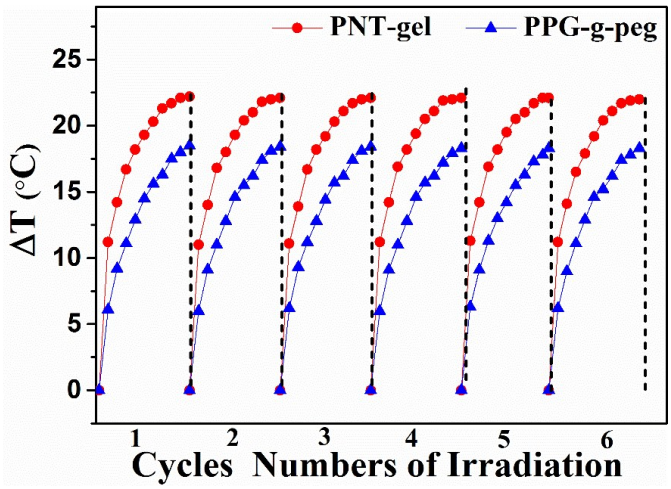

Figure S9. Elevated temperature profiles of PPG-g-peg and PNT-gel over six cycles of NIR exposure (808 nm, 0.28 W cm^{-2}).

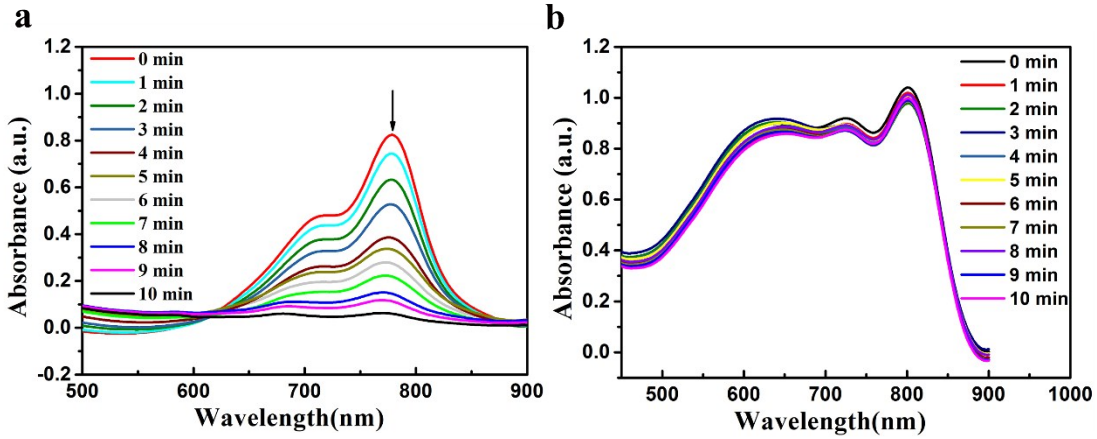

Figure S10. UV-vis-NIR absorbance spectra of (a) free ICG and (b) ICG/PPG-g-peg complex solution under 808 nm laser at 0.28 W cm^{-2}.

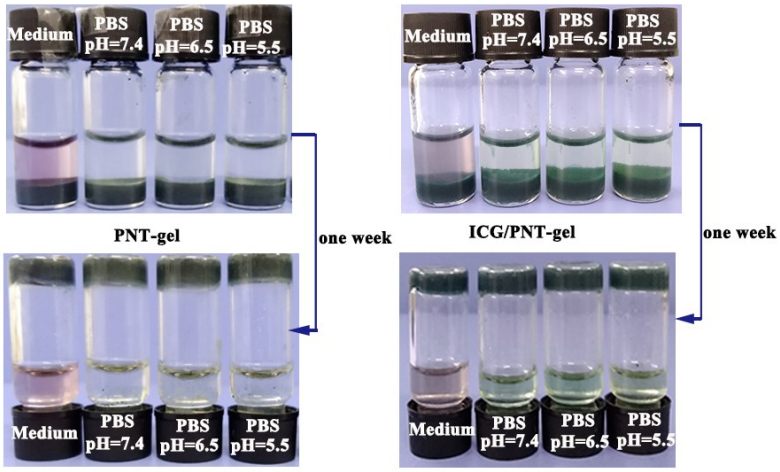

Figure S11. Stability of PNT-gel in different solutions (including RPMI-1640 medium and PBS with different pH values, measured at ambient temperature).

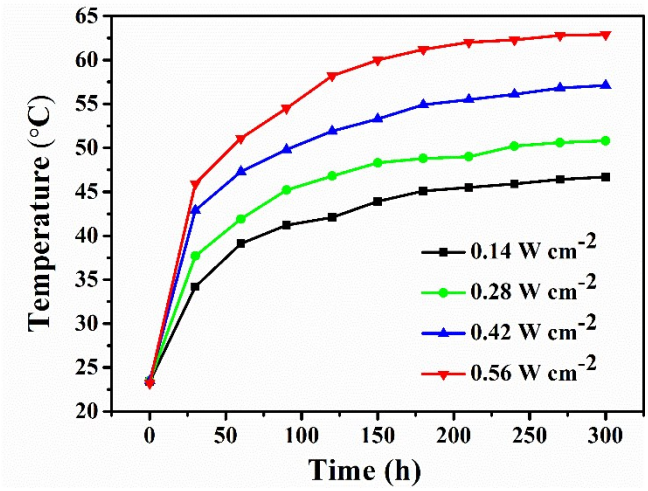

Figure S12. Temperature elevation curves of PNT-gel under different laser power irradiation, as a function of irradiation time.

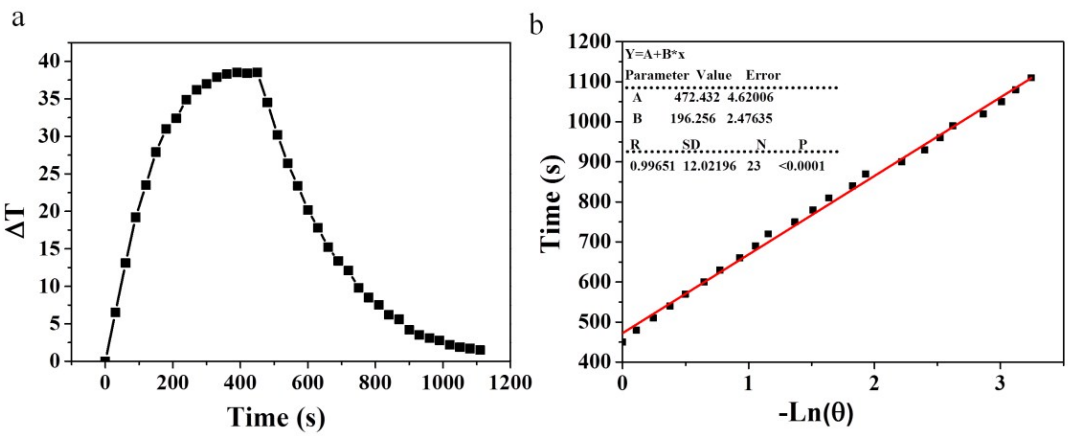

Figure S13. The photothermal conversion efficiency (η) of PPG-g-peg photothermal backbone. (a) The photothermal response of the PPG-g-peg aqueous solutinon (40 mg mL^{-1}) for 450 s with a NIR laser (808 nm, 1.0 W cm^{-2}) and then the laser was shut off. (b) Linear time data versus – ln θ obtained from the cooling period of Fig. S13a.

$$\eta = \frac{hA\Delta T_{max} - Q_S}{I(1 - 10^{-A_\lambda})} \qquad (1)$$

h is the heat transfer coefficient, A is the surface area of the sample container, ΔT_{max} is the maximum temperature change, Qs is the heat associated with the light absorbance

of pure water. I is the laser power, and A_λ is the absorbance value at 808 nm. θ is the ratio of ΔT to $\Delta Tmax$, which is introduced to get the value of hA:

$$\theta = \frac{\Delta T}{\Delta T_{max}} \qquad (2)$$

Where ΔT is defined as T - T_{surr} (T and T_{surr} are the sample temperature and ambient temperature, respectively). Thus, hA can be determined as following:

$$hA = \frac{mC_p}{\tau} \qquad (3)$$

τ is the slope of the linear time data from the cooling period *vs* - lnθ. m and C_p are the mass and heat capacity of water, respectively.[3]

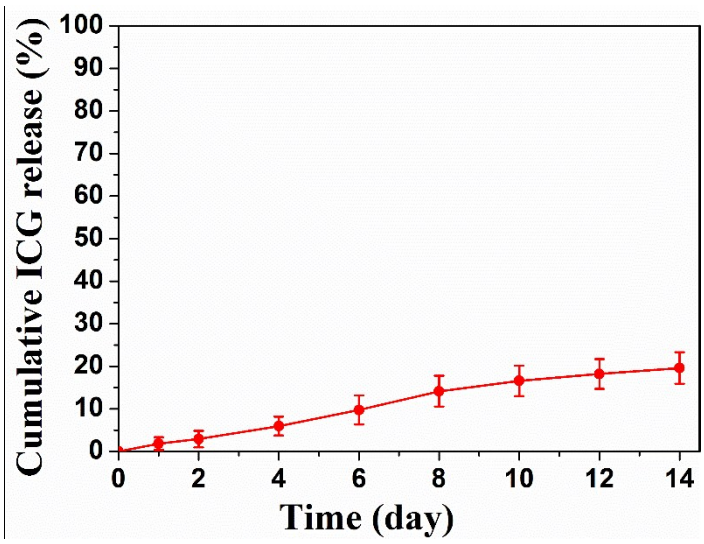

Figure S14. Release profiles of ICG from ICG/PNT-gel in PBS (n = 5).

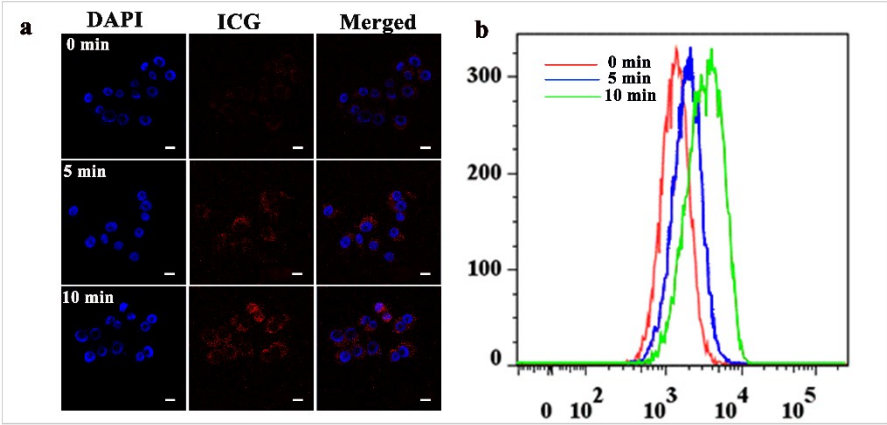

Figure S15. The in vitro NIR-controlled ICG release and cellular uptake behavior. (a) confocal microscopic images of 4T1 cells incubated with ICG/PNT-gel following NIR-light irradiation for 0 min, 5 min and 10 min, respectively. Red fluorescence represented ICG. Cell nucleus (blue) were stained with DAPI. (scale bar = 20 μm) (b) The corresponding fluorescence intensity of ICG inside 4T1 cells determined by flow cytometer.

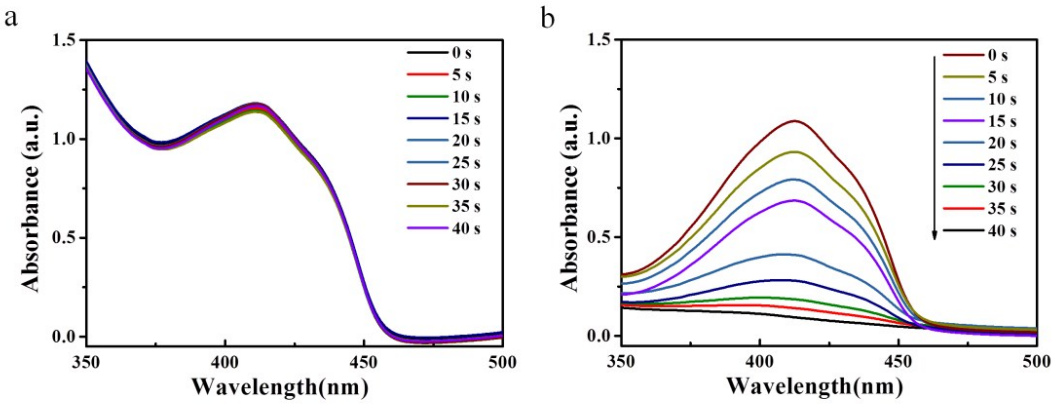

Figure S16. UV-Vis spectra of (a) PPG-g-peg+DPBF and (b) ICG+DPBF under different irradiation times with 808 nm laser (0.28 W cm^{-2}).

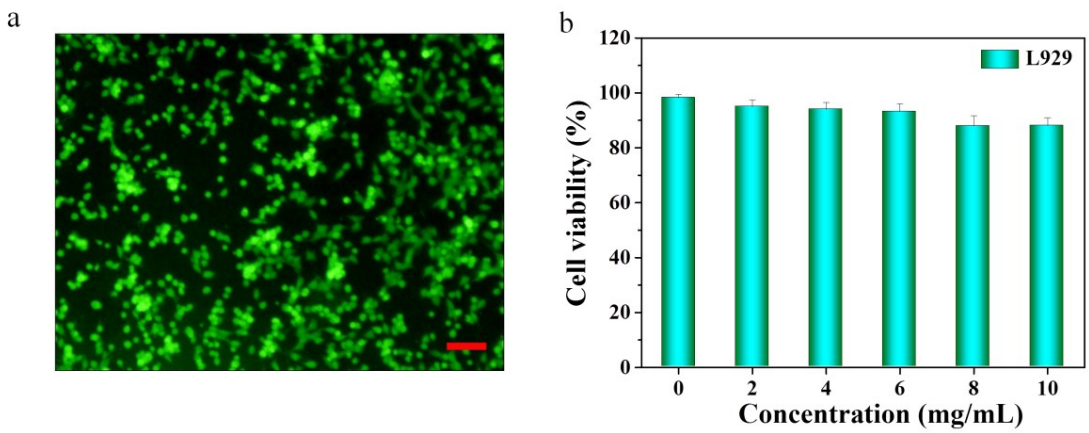

Figure S17. The biocompatibility of the PNT-gel **(**a) Live/Dead staining assay of PNT-gel on L929 cells at the concentration of 10 mg/mL. Scale bar: 100 μm. (b) Quantitative detection of cells viability after incubated with different concentration of PNT-gel.

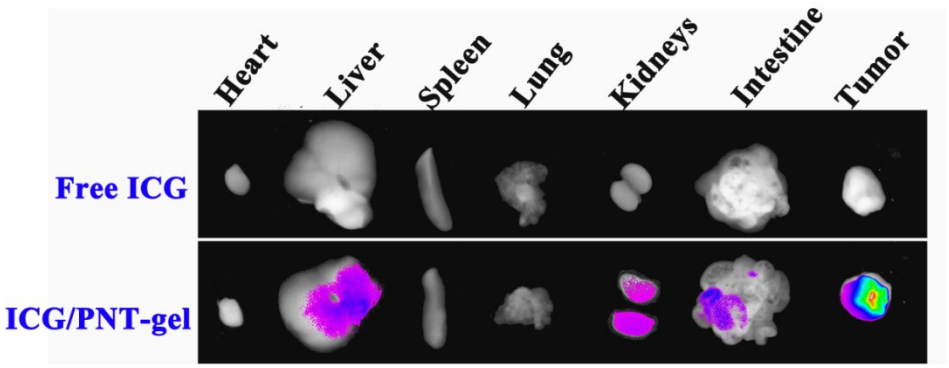

Figure S18. *Ex vivo* NIR fluorescence images of major organs and tumors obtained after 14 days of the administration of free ICG solution and ICG/PNT-gel.

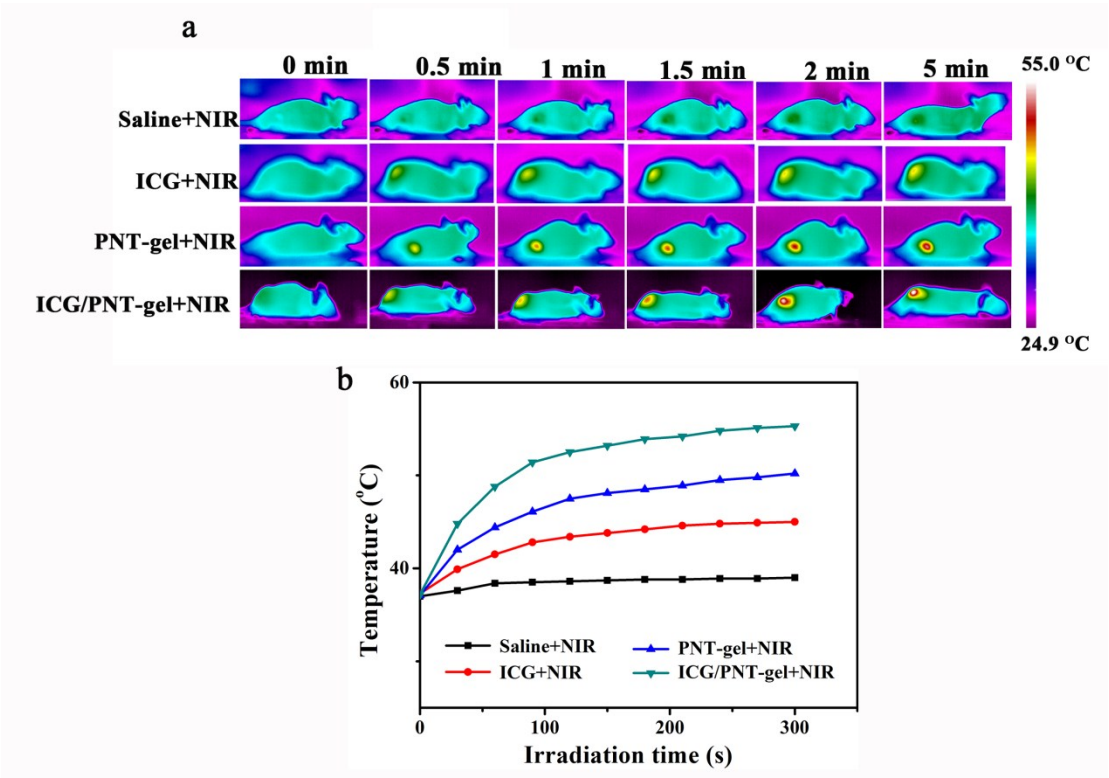

Figure S19. The photothermal effect of PNT-gel *in vivo* (a) Infrared thermal images of 4T1 tumor-bearing mice after intratumorally injection with single dose of different formulation and following exposure to an 808 nm laser, taken at the first day. (b) the corresponding maximum temperature profiles of the irradiated area.

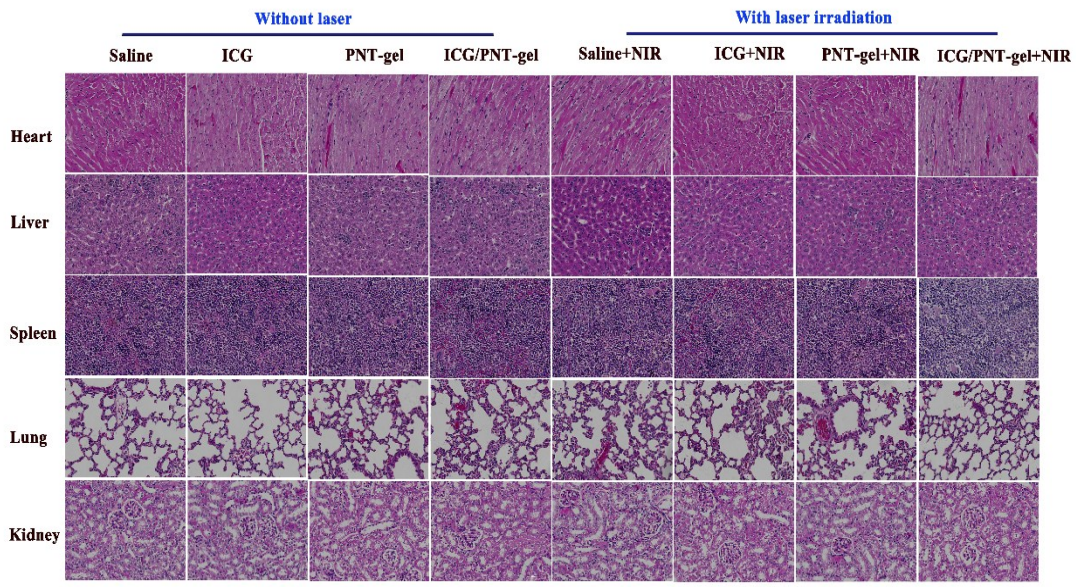

Figure S20. Histopathological images of the major organs including heart, liver, spleen, lung, and kidney harvested from the mice after 14-days treatment.

References:

[1] Y. Duan, Q. Tang, Y. Chen, Z. Zhao, Y. Lv, M. Hou, P.Z. Yang, B.L. He and L.M. Yu, *J. Mater. Chem. A,* 2015, 3, 5368-5374.

[2] W. Ha, X.B. Zhao, K. Jiang, Y. Kang, J. Chen, B.J. Li and Y.P. Shi, *Chem. Commun.,* 2016, 52, 14384-14387.

[3] J. Zhou, Z. Lu, X. Zhu, X. Wang, Y. Liao, Z. Ma and F.Y. Li, *Biomaterials,* 2013, 34, 9584-9592.